IEEE Access
Multidisciplinary | Rapid Review | Open Access Journal

Received 5 February 2024, accepted 25 February 2024, date of publication 4 March 2024, date of current version 8 March 2024.

Digital Object Identifier 10.1109/ACCESS.2024.3372601

RESEARCH ARTICLE

Thermal Characteristic and Analysis of Electro-Hydrostatic Actuator

JIAHUI LIU, HAO HUANG, YAOWEN GE, XIAOLI ZHAO, WENXIANG DENG, GUANGFA GAO, AND JIANYONG YAO, (Member, IEEE)
School of Mechanical Engineering, Nanjing University of Science and Technology, Nanjing 210094, China

Corresponding author: Jianyong Yao (jerryyao.buaa@gmail.com)

This work was supported in part by the National Key Research and Development Program of China under Grant 2021YFB2011300; in part by the National Natural Science Foundation of China under Grant 52305063 and Grant 52205062; and in part by the Natural Science Foundation of Jiangsu Province, China, under Grant BK20220950.

ABSTRACT Electro-hydrostatic actuators (EHAs) are widely utilized due to their superior integration and high power-to-weight ratio. However, the elimination of a centralized oil source in EHAs restricts the cooling capacity of the system, leading to potential adverse effects on performance and longevity caused by excessively elevated temperatures. This study meticulously investigates the power loss during energy transfer and the heat dissipation properties of EHAs. To further study the heat behavior, a one-dimensional simulation model of the EHA thermal-hydraulic system is developed. By comparing the simulation results with experimental data obtained from an actual EHA system, the good agreement between the simulation and experimental results confirms the accuracy of the model in predicting the thermal performance of EHAs. Based on the validated model, different cooling schemes for EHAs is further explored. The cooling mechanisms of air cooling and phase change heat dissipation are considered to enhance heat dissipation and manage the temperature rise within the EHA. This study provides insights and guidance for the early-stage thermal design of EHAs, aiming to optimize system performance and prolong its operational life.

INDEX TERMS Electro-hydrostatic actuator, thermal-hydraulic model, heat transfer, cooling performance.

I. INTRODUCTION

The emergence of multi-electric airplanes has indeed generated significant interest and research in electro-hydrostatic actuator (EHA) systems [1]. EHAs are known for their exceptional attributes, such as high power density, reliability, and compactness. These characteristics have established EHAs as the preferred choice for modern aircraft [2], [3]. Moreover, EHAs are increasingly being employed in various other industrial applications like wind turbines [4], transport [5], [6], and exoskeleton robots [7], [8]. The elimination of a centralized hydraulic tank in EHAs can result in heat accumulation within the system. The heat generated during energy transfer and conversion must be dissipated through the limited cooling capacity of the structure's surface. leading to elevated temperatures within the EHA [9]. These heightened temperatures can adversely impact the performance of the hydraulic oil, initiating a detrimental cycle of increased overheating with a significant loss of viscosity, thinning of the hydraulic oil, increased flow loss, and increased wear on the system components. In addition, high temperatures accelerate the oxidation of the fluid and deterioration of seals, reducing the oil lifespan, diminishing system performance, and potentially even seriously affecting the healthy operation of the EHA [10], [11].

In recent years, a number of studies have focused on EHA systems to improve cooling capacity, reduce heat generation, and optimize energy efficiency. Researchers have made significant advancements in enhancing the structure of EHA components. An inventive configuration, known as a wet Permanent Magnet Synchronous Motor (PMSM) is designed with both the stator and rotor immersed in aviation hydraulic fluid, which improves the heat dissipation performance of the PMSM [12], [13]. Chao [14] designed a load-sensitive mechanism hydraulic pump specifically for EHAs. In this design, the volumetric displacement automatically decreases

The associate editor coordinating the review of this manuscript and approving it for publication was Mouloud Denai.

as the load pressure increases, effectively reducing peak torque requirements and minimizing motor heat generation. Researchers also explored various strategies to optimize EHA configuration and power matching. Song et al. [15] proposed a direct load-sensing EHA (DLS-EHA) featuring a load-sensing pump. By adjusting the pump displacement automatically based on the load pressure, this system aims to reduce motor heating and achieve a certain degree of motor-pump power matching. Huang et al. [16] proposed the concept of an active load-sensitive EHA (ALS-EHA), which dynamically adjusts the pump displacement in response to the load pressure, enabling adaptive regulation and optimization of the power matching process. Yang et al. [17] applied the non-dominated sequential genetic algorithm with elite strategy (NSGA-II) to intelligently optimize key parameters in EHAs, facilitating the optimal matching of system performance. Moreover, Shang et al. [18] proposed a new energy recovery EHA (ER-EHA) that enhances system efficiency by eliminating power loss, reducing motor heating, shrinking system size, and improving the power-to-weight ratio of the system via a hydraulic energy recovery unit.

To comprehensively address the heat dissipation challenge, relying solely on structural and algorithmic enhancements is insufficient to mitigate the heat generated by EHAs. Consequently, it becomes imperative to conduct a detailed analysis of the heat generation from individual EHA components. This analysis serves as the foundation for developing tailored heat dissipation strategies for different components within the EHA system. Han et al. [19] proposed a thermally coupled EHA model that integrates lumped-parameter modeling and Computational Fluid Dynamics (CFD) methods to conduct simulation analysis under key temperature conditions. Yang et al. [20] established the thermal balance equations for the EHA system by lumped-parameter method and established a multidisciplinary model encompassing flow and thermal fields to study the temperature changes during operation. Yan et al. [21] analyzed the heat generation in electrohydraulic servo pump control system, established the thermal power model in the system, and conducted the thermal balance analysis of the system based on ANSYS and AMESim. However, the modeling of the above studies is complicated and the simulation requires more parameters that are difficult to obtain. Qu et al. [22] simplified intricate heat transfer processes to evaluate the cooling demand of EHAs. Ketelsen et al. [23] developed a lumped thermal-hydraulic model validated based on EHA experimental data, suitable for the early design stage of the system with only limited information. To address thermal dissipation challenges and enhance compactness in EHAs, researchers have explored various approaches. The A380 [24] incorporates an improved design of the wings to ensure more convective air cooling. Lenoble et al. [25] conducted thermal analysis of an in-cavity EHA under critical flight conditions to support and optimize the motor design for effective manage thermal issues. Li et al. [26] proposed a novel ribbed honeycomb heat sink (RHCS) for EHAs to demonstrate better thermal performance and lighter mass.

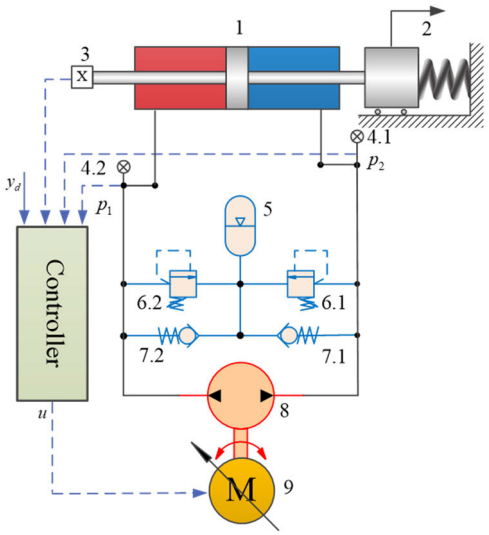

FIGURE 1. The EHA system schematic diagram. 1: actuator; 2: load; 3: displacement sensor;4: pressure sensor; 5: accumulator; 6: relief valve; 7: check valve; 8: hydraulic pump; 9: servomotor.

Inspired by the previous literature and considering the trade-off between accuracy and modeling complexity, this study aims to propose an EHA thermal-hydraulic model based on the lumped-parameter approach. The objective is to provide a quick estimation of system temperature with minimal effort and prior information, facilitating swift assessments and decision-making processes related to EHA thermal management. The key contributions of this study include: 1) The investigation of power loss and heat dissipation characteristics specific to each component involved in the energy transfer process within the EHA. 2) A one-dimensional simulation model of the EHA thermal-hydraulic system is developed, enabling a rough prediction of system temperature through comparison of simulation results with the experimental data. 3) Cooling mechanisms of air cooling and phase change cooling are considered to enhance heat dissipation and manage the temperature rise within the EHA.

The remaining parts of this paper are elaborated as follows. Section II briefly illustrates the basic theory of the EHA system based on power loss modeling. Section III describes the simulation model and dynamic simulation of the EHA system, and then compares and validates it with the actual experimental data, and Section IV describes the cooling scheme based on the thermal simulation model. Finally, Section V concludes and provides perspectives for future work.

II. THERMAL HYDRAULIC MODEL

A. STRUCTURE AND PRINCIPLE

The EHA system studied in this paper adopts a fixed displacement hydraulic pump and variable speed motor (FPVM) type scheme.

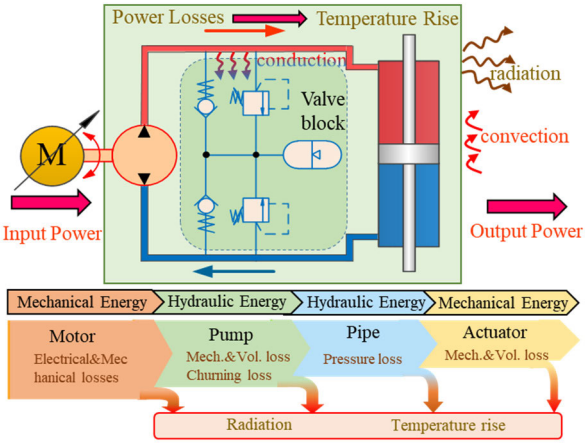

FIGURE 2. System energy transfer process and power loss.

The system configuration, as illustrated in Fig.1, integrates a servomotor, a bi-directional piston pump, a hydraulic cylinder, an accumulator, relief valves, sensors, and a controller. The core of the system is a servo motor connected to a piston pump via a coupling. The flow rate of the pump is regulated and controlled by changing the speed of the servomotor. The differential pressure in the chamber leads to a direct drive of the double-rod symmetrical hydraulic cylinder, which drives the external loads. To maintain proper operation, an accumulator is incorporated into the system. This accumulator serves to fill the low-pressure side via a check valve, ensuring a continuous supply of hydraulic fluid. Additionally, two relief valves are employed as safety mechanisms to keep the system pressure within the maximum permissible range. The sensors in this system are used to monitor the status of the hydraulic cylinders such as pressure and displacement. The controller is responsible for accurately controlling the position and movement of the servomotor.

B. POWER LOSS MODEL

In the EHA system, the main function of the motor is to convert electrical energy into mechanical energy to rotate the pump; the pump is to output the flow rate through the bi-directional movement of the motor, which ultimately controls the movement of the cylinder and converts the mechanical energy into the pump; and the actuator is to convert the hydraulic energy into the mechanical energy to push the load to move. The energy transfer process and power losses in an EHA system are shown in Fig. 2. In the process of energy conversion and transfer, various losses generated by the EHA are converted into internal energy, which is stored in the components and transmission medium, leading to an increase in system temperature.

1) MOTOR

The power loss of the motor can be categorized into electrical and mechanical losses [27]. Electrical losses are mainly winding copper loss and stator iron loss. The winding copper losses caused by the passage of current through a copper conductor produce the thermal effect. According to Joule's law, the winding copper loss P_{cu} can be expressed as

$$P_{cu} = mI^2R \tag{1}$$

where m is the number of phases of the motor winding; I is the RMS current; R is the phase resistance.

Stator iron loss is an important part of electrical loss. According to Bertotti's iron loss model, different generation mechanisms categorize iron loss into hysteresis loss, eddy current loss, and additional loss. Stator iron loss P_{Fe} can be described as:

$$P_{Fe} = \mathrm{k}_h f B_m^2 + \mathrm{k}_c f^2 B_m^2 + \mathrm{k}_e f^{1.5} B_m^{1.5} \tag{2}$$

where k_{h} is the hysteresis loss coefficient; k_{c} is the eddy current loss coefficient; k_{e} is the additional loss coefficient; B_{m} is the magnitude of magnetic flux density; f is the frequency of the alternating magnetic field; α is an empirical coefficient.

The mechanical loss of PMSM mainly comes from friction. The rotor rotates at high speed with the air in the gap can produce friction loss, which is negligible due to the loss of power is too small; Motor bearing friction loss is incurred in high-speed rotation, the formula is as follows

$$P_{mc} = k_m M_m \omega \tag{3}$$

where k_{m} is the bearing friction loss coefficient; M_m is the bearing load; w is the speed.

Numerous studies have shown that the permanent magnet eddy current loss, rotor iron loss, and mechanical loss of PMSMs are much smaller compared to the stator iron loss and winding copper loss under most operating conditions. According to the above analysis, the total heat generation power of the motor can be given by:

$$P_{motor} = P_{cu} + P_{Fe} \tag{4}$$

2) HYDRAULIC PUMP

The loss of the piston pump includes volume loss and mechanical loss [21], [28]. Volume loss is mainly the energy loss caused by the leakage of oil through the gap, the leakage path of a piston pump consists of the piston pair, the slipper pair, and the port pair. Mechanical loss is divided into friction loss and churning loss. Friction loss refers to the energy loss that occurs due to the contact between the moving parts and the pump body; churning loss is the energy loss caused by the eddy current and turbulence generated by the oil in the pump chamber.

The heat generation power of the leakage between the piston and the cylinder bore P_{z} can be expressed as:

$$P_z = N \frac{\pi d_z \Delta p_z^2}{12 \mu L_z} \delta_z^3 (1 + 1.5e^2) \tag{5}$$

where N is the number of pistons of the piston pump; d_{z} is the piston diameter; Δp_{z} is the pressure difference between the front and rear piston pair; μ is the oil dynamic viscosity;

L_z is the sealing length of the piston pair; δ_z is the oil film thickness; e is eccentric ratio.

The heat generation power of the leakage between the slipper parts and the plate P_h can be expressed as:

$$P_h = N\frac{\pi\delta_h^3\Delta p_h^2}{6\mu\ln(r_2/r_1)} \tag{6}$$

where δ_h is the oil film thickness; Δp_h is the pressure difference between the slipper pair; r_1 and r_2 are the inner and outer radius of the sealing belt of the slipper, respectively.

The heat generation power of the leakage between the flow distribution shaft and the rotor P_p can be expressed as:

$$P_p = \frac{\varphi_p r_p \delta_p^3 \Delta p_p^2}{12\mu L_p} \tag{7}$$

where ϕ_p is the leak angle; r_p is the radius of the flow distribution shaft; δp is the oil film thickness; Lp is the contact length.

Mechanical losses mainly come from friction and churning, the formula is as follows.

$$P_m = \eta_m M_p \omega \tag{8}$$

where η_m is the mechanical loss coefficient; M_p is the load.

The churning losses due to rotation mainly at low speeds are negligible in this experiment. Therefore, the total heat generation power of the piston pump can be expressed as:

$$P_{pump} = P_z + P_h + P_p + P_m \tag{9}$$

3) PIPE AND ACTUATOR

Hydraulic pipes in EHA systems are often designed as valve blocks, loss of power can be attributed to pressure losses. As hydraulic fluid flows through the lines, the friction between the flowing fluid and the inner surfaces of the pipes causes energy to be dissipated in the form of heat. Additionally, localized losses can occur within the hydraulic system. These losses are caused by turbulence resulting from sudden changes in flow velocity or shocks. This turbulence leads to further energy dissipation and generates additional heat. The heat generation power of the hydraulic pipe P_{pipe} is shown as follows.

$$P_{pipe} = (\sum \lambda \frac{l_{pipe}}{d_{pipe}} \frac{\rho v^2}{2} + \sum \xi \frac{\rho v^2}{2}) q_{pipe} \tag{10}$$

where λ is the resistance coefficient along the pipe; ρ is the density of hydraulic oil; v is the hydraulic fluid flow rate; l_{pipe} is the length of the pipe; d_{pipe} is the diameter of the pipe; ξ is the local loss coefficient, and q_{pipe} is inlet flow of the pipe.

The power loss of the actuator can be attributed to friction and leakage losses, with leakage losses being the main concern. The heat generation power of the hydraulic actuator P_{ac} is shown as follows.

$$P_{ac} = \Delta p_{ac} q_{cl} \tag{11}$$

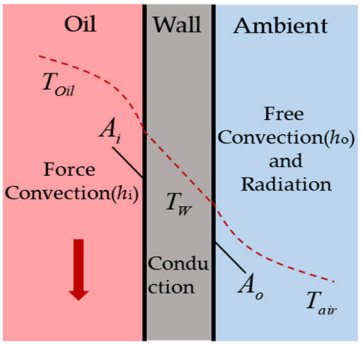

FIGURE 3. The process of heat exchange.

TABLE 1. Dimensionless parameter.

Parameter	Formula
Nusselt (Nu)	$\mathrm{Nu} = \frac{hl_c}{k_f}$
Prandtl (Pr)	$\mathrm{Pr} = \frac{\mu c_p}{k_f}$
Reynolds (Re)	$\mathrm{Re} = \frac{vd}{v}$
Grashof (Gr)	$\mathrm{Gr} = \frac{gl_c^3\beta_{air}\Delta T}{v^2}$

l_c = characteristic length

where Δp_{ac} is the pressure difference between the actuator and q_{cl} is leakage flow.

C. HEAT TRANSFER AND DISSIPATION

The heat transfer and dissipation model provides a comprehensive description of the heat exchange process [29]. Fig. 3 represents this heat transfer process, depicting three distinct layers: the red area corresponds to the oil, the blue area represents the air, and the center represents the wall. According to this model, it is assumed that all elements within the system undergo heat transfer through forced convection. Forced convection refers to the process by which heat is transferred between the oil and the inner wall due to the motion of the fluid. The flow of the fluid carries thermal energy from the oil temperature (T_{oil}) towards the inner wall (A_i). Once the heat is transferred to the inner wall via forced convection, it further propagates through the element walls via conduction. Finally, heat is dissipated from the outer wall (A_o) of the element to the ambient air (T_{air}) through free convection and radiation. Some of the necessary dimensionless parameters are shown in Table 1.

1) CONVECTION

The process of heat transfer between the fluid and the solid wall surface is called convective heat transfer. Convection is a distinct mode of heat transfer that occurs in liquids and gases. The convection process in the inner wall of a hydraulic element is assumed to be forced convection, and the convection

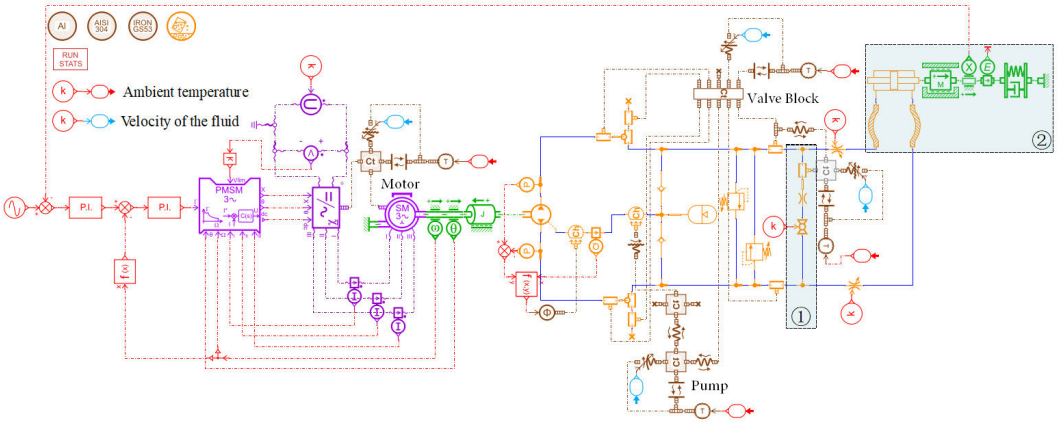

FIGURE 4. Schematic diagram of the EHA thermal-hydraulic model.

process in the outer wall is regarded as free convection. The convection heat transfer ϕ_1 can be expressed as:

$$\phi_1 = hA_s\Delta T_1 \tag{12}$$

where h is the convection coefficient, which can be divided into the inner and outer heat transfer coefficients h_i and h_o; A_s is the heat transfer area, which can be divided into the inner and outer heat transfer area A_i and A_o; ΔT_1 is the temperature difference between the solid surface and the fluid; d_i and d_o are the inner and outer diameter of the cylinder, respectively; L is the element length; a is the side length of the cube-shaped modeled components. The convection coefficient between the wall and the fluid is calculated from the Nusselt number. The formulas for different conditions are given below.

Forced convection in a cylinder (physical characteristics at oil temperature, $\mathrm{T_{oil}}$)

- Laminar: $l_c = d_i$,$\mathrm{Pr_w}$ =Pr($\mathrm{T_w}$), Re < 2300

$$\mathrm{Nu} = [3.66^3 + 0.7^3 + (1.615\sqrt[3]{\frac{\mathrm{Re}\cdot\mathrm{Pr}\cdot d_i}{L}} - 0.7)^3]^{\frac{1}{3}} \times (\frac{\mathrm{Pr}}{\mathrm{Pr}_w})^{0.11} \tag{13}$$

- Turbulent: $l_\mathrm{c} = d_\mathrm{i}$, $\mathrm{Pr_w}$ =Pr($\mathrm{T_w}$), Re > 10000

$$\mathrm{Nu} = \frac{\frac{(Re-1000)\mathrm{Pr}}{8(1.82\log(\mathrm{Re})-1.64)^2}[1+(\frac{d_i}{L})^{\frac{2}{3}}]}{1+12.7(\mathrm{Pr}^{\frac{2}{3}}-1)\sqrt{0.125(1.82\log(\mathrm{Re})-1.64)^{-2}}} \times (\frac{\mathrm{Pr}}{\mathrm{Pr}_w})^{0.11} \tag{14}$$

Free convection to air (physical characteristics at $0.5(T_\mathrm{w}+T_{air})$)

- Horizontal cylinder: $l_\mathrm{c} = d_\mathrm{o}$, Gr =Gr($T_\mathrm{w}$-$T_\mathrm{air}$)

$$\mathrm{Nu} = \left\{0.6 + \frac{0.387\mathrm{Gr}\cdot\mathrm{Pr}^{\frac{1}{6}}}{\left(1+\left(\frac{0.559}{\mathrm{Pr}}\right)^{\frac{9}{16}}\right)^{\frac{8}{27}}}\right\}^2 \tag{15}$$

- Cube: $l_\mathrm{c} = A_\mathrm{o}/(4\mathrm{a}^3)$, Gr =Gr($T_\mathrm{w}$-$T_\mathrm{air}$)

$$\mathrm{Nu} = 5.748 + 0.752\left\{\frac{\mathrm{Gr}\cdot\mathrm{Pr}}{\left[1-\left(\frac{0.492}{\mathrm{Pr}}\right)^{\frac{9}{16}}\right]^{\frac{16}{9}}}\right\}^{0.252} \tag{16}$$

2) CONDUCTION

Conduction is the transfer of energy from the high-temperature part of an organism to the low-temperature part by the molecular thermal motion of a large number of substances inside the system. Heat conduction is the main mode of heat transfer in solids, and the heat conduction ϕ_2 can be expressed as follows according to the conditions:

- Pipe:

$$\phi_2 = 2\pi kL_{pipe}\frac{\Delta T_2}{\ln(d_o/d_i)} \tag{17}$$

- Cube:

$$\phi_2 = ka^2\frac{\Delta T_2}{L_w} \tag{18}$$

where k is the thermal conductivity of the material. ΔT_2 is the temperature difference between the walls.

3) RADIATION

Radiation is the transfer of energy from an element by emitting radiant energy through electromagnetic waves. Thermal radiation is an intrinsic property of an element. Thermal radiation ϕ_3 can be expressed as follows:

$$\phi_3 = \sigma\varepsilon A_0\left(T_w^4 - T_{\mathrm{air}}^4\right) \tag{19}$$

where ε is the emissivity; σ is the Stefan-Boltzmann constant ($5.67\cdot10^{-8}\mathrm{W/(m^2K^4)}$).

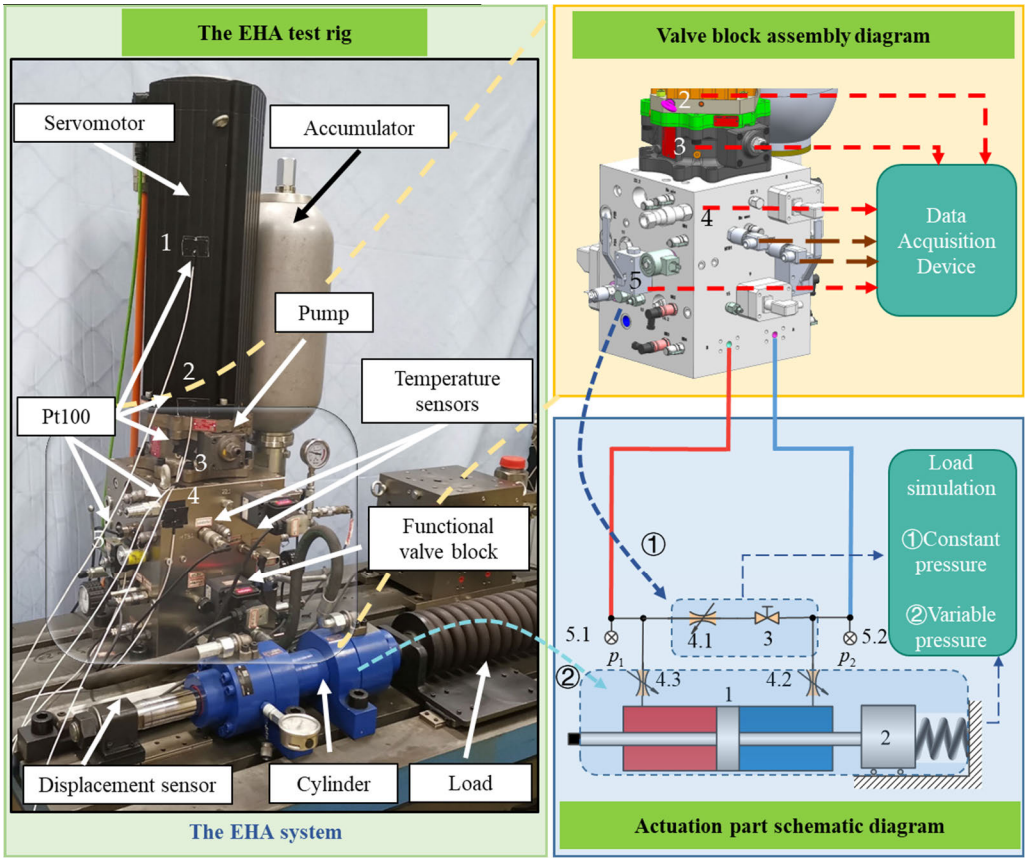

FIGURE 5. The EHA system test schematic diagram and test rig. 1: actuator; 2: load; 3: ball valve; 4: needle valve; 5: pressure sensors.

TABLE 2. Parameters of the simulation model.

Parameter	Value	Parameter	Value
Displacement	19cm^3/rev	Mass of valve block	190kg
Diameter of piston	63mm	Mass of motor	75kg
Diameter of the rod	45 mm	Mass of pump	20kg
Stroke	±50mm	Area of the valve block	0.44m^2
Winding resistance at 25 °C	0.074Ω	Area of motor	0.5m^2
Maximum current	340.5A$_{rms}$	Area of pump	0.1m^2
Winding inductance	1.433mH	Hydraulic oil	ISO VG 46 oil

TABLE 3. Specification of test rig components.

Name	Specification
EPU	MoogSEPU019ADN1H0C
Industrial computer	Advantech Industrial IPC-610
Pressure sensors	MEAS US175-C00002-200BG
Efficient ram area	1526.81 mm^2
Stroke	100mm
Spring stiffness	245N/mm
Spring damping	15N/(mm/s)
Mass load	13.5kg
Hydraulic oil	ISO VG 46 oil
Thermal camera	Hikvision
Linear encoder	Heidenhain LC485
Counter module	Heidenhain IK-220
A/D converter module	Advantech PCI-1716
D/A converter module	Advantech PCI-1723

D. ONE-DIMENSIONAL(1D) THERMAL MODEL

A thermal-hydraulic model of the EHA system is developed in AMESim for system simulation and temperature rise analysis, as depicted in Fig. 4. The model consists of four sub-models: a PMSM motor, a hydraulic pump, pipelines, and valve block, an actuator, and heat dissipation model. The model incorporates leakage gap, spring stiffness, and damping to mimic the actual working conditions. The modeling process involves two assumptions: 1) The initial temperature is equal to the ambient temperature, and the ambient temperature remains constant during the test; 2) The heat transfer coefficient is approximated based on the material and the dominant mode of heat transfer. The parameters used in the simulation model are shown in Table 2.

III. RESULTS

A. EXPERIMENTAL PLATFORM OF EHA

The EHA system test rig in a laboratory environment is shown in Fig. 5. The unit consists of an electro-hydrostatic pump unit

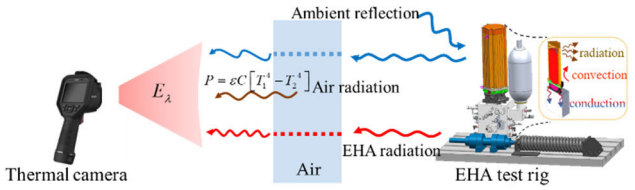

FIGURE 6. The process of thermal data acquisition.

(EPU), which consists of a permanent magnet synchronous servomotor and a piston pump. In addition, it consists of a hydraulic cylinder, a load mass, a compression spring, a linear encoder, pressure sensors, temperature sensors, a data acquisition device, and an industrial computer. The component specifications of the EHA are shown in Table 3.

To collect the system signals under different operating conditions, temperature data were obtained by testing on the experimental platform. This experiment is carried out in two separate cases:

① Closing the needle valves (4.2) and (4.3), the motor at a constant speed, opening the ball valve (3), and adjusting the needle valve (4.1). Open the needle valve (4.1) to different degrees to simulate different pressure loads.

② Closing the ball valve (3) and opening the needle valves (4.2) and (4.3), the system is closed-loop controlled and the hydraulic cylinder is capable of compressing the spring movement to achieve variable loads.

Since both the ball and needle valves are inserted inside the valve block, the experimental setup is not only installed for the thermal behavior of the various sensors prepared for the measurement but also for thermal resistors to assist in measuring the surface temperatures at the points shown in Fig. 5. Among them: Point 1: the center of the motor body surface; Point 2: the combination of the hydraulic pump and the motor; Point 3: the center of the hydraulic pump body surface; Point 4: the main valve block surface; Point 5: the center of the ball valve block surface. The thermal camera data was collected at the same time. The thermal data acquisition process is shown in the Fig.6.

B. SIMULATION AND EXPERIMENTAL RESULTS COMPARISON

The simulation time settings are consistent with the experiments, and the simulation results of the dynamic performance of the thermal-hydraulic model in Case 1 and Case 2 are obtained.

Case 1: The experiment is conducted at an ambient temperature of 16°C and the motor speed is 500rpm, the thermal image and thermal resistance data are obtained under various pressures (the needle valve (4.1) differential pressure was set to 0bar, 20bar, 40bar, and 60bar, respectively). Fig. 7 shows the thermal images at 60 bar pressure. The comparison of thermal camera data and thermal resistance data indicates that the temperature at Point 2 (the combination of the hydraulic pump and the motor) is comparable to the temperature at

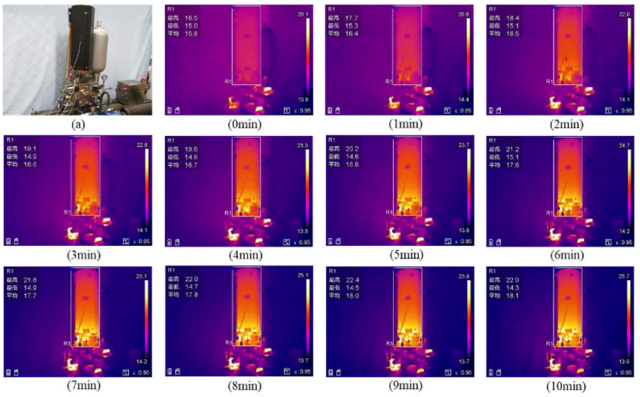

FIGURE 7. Thermal image in 10 minutes under 60 bar pressure.

Point 3 (the center of the hydraulic pump body surface). Due to the difficulty of simulating the combination area in the 1D lumped model, the temperatures at Points 1, 3, 4, and 5 of the model are extracted. The ambient temperature is set to 16°C in the simulation model, loaded with 0 bar, 20 bar, 40 bar, and 60 bar respectively, and the heat dissipation mode is assumed to be free convection. The comparison of the experimental thermal resistance data and the results of the simulation are presented in Fig. 8.

The simulation results demonstrate a strong agreement with the experimental data. The ball valve and needle valve block, which simulate the pressure variation, exhibit the significant temperature changes since the pressure loss in this area is entirely converted into thermal energy. Some of this energy increases the internal energy of the hydraulic oil, while the rest is dissipated as heat this separate valve block. The main valve block, due to its larger size and higher thermal resistance, experiences a less pronounced temperature rise. The temperature variations observed on the surfaces of the motor and hydraulic pump align with the power loss analysis and represent the primary heat sources within the system. The hydraulic pump displays more substantial temperature changes, attributed to its lower low-speed efficiency and smaller heat transfer area. During simulation, we observed that the temperature extracted directly from the hydraulic pump model outlet is higher than the temperature measured experimentally. As shown in Fig. 9, we analyzed the structure and found that the temperature sensor is located at the end of the manifold, which is distant from the main circuit, and the temperature fluctuation primarily arises from oil heat transfer. Hence, we modified the model to obtain the simulation temperature here and the temperature sensor results, as shown in Fig. 10, and we consider that such an improvement is deemed reasonable.

Case 2: The ambient temperature of the experiment is 26.4°C. In this case, the EHA system is controlled by a closed-loop scheme with position feedback, and the state data are recorded under a sinusoidal signal (with an amplitude of 20 mm and a frequency of 0.2 Hz). The thermal-hydraulic

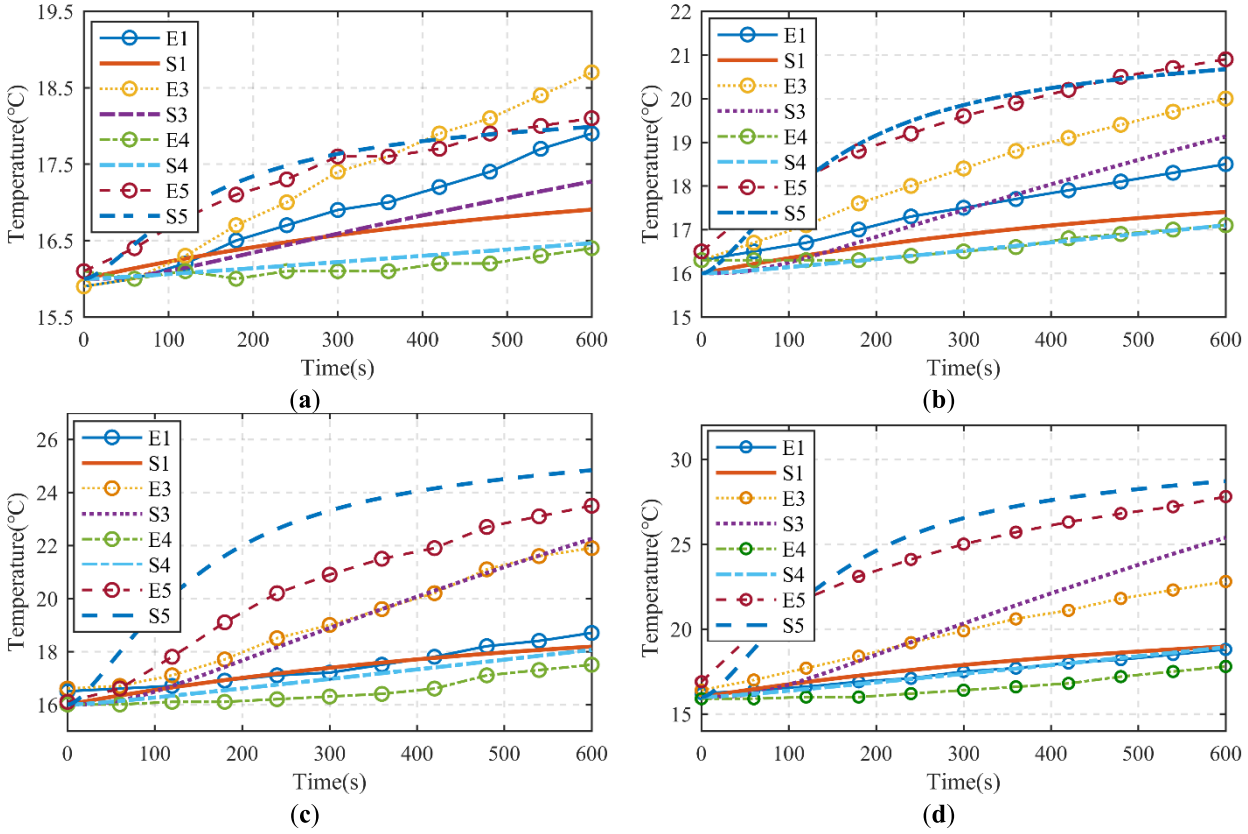

FIGURE 8. The comparison between the experimental thermal resistance data and the results of simulation at different pressures: (a) 0 bar; (b) 20 bar; (c) 40 bar; (d) 60 bar. 'E' is the experimental data and 'S' is the simulation data.

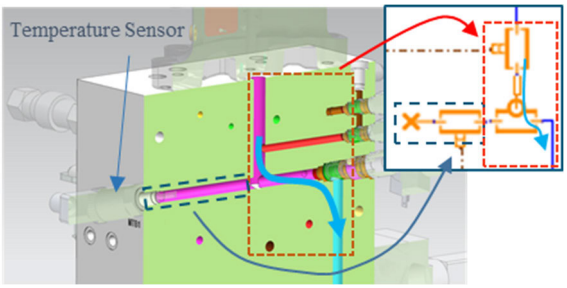

FIGURE 9. The internal structure of the main valve block.

system model is given the same command signal to achieve the position tracking of the piston of the hydraulic cylinder. The heat dissipation mode is considered to be free convection. Fig. 11 illustrates the experimental and simulation results.

The simulation results indicate that the thermal-hydraulic model is effectively replicates the actual operating condition under the sinusoidal command. The spurs in the experimental pressure and force curves are attributed to the realistic nonlinear friction. To facilitate the computational solution, the model is set up with only viscous friction, which has minimal impact on the overall thermal behavior.

The simulation results in different cases demonstrate that the thermal-hydraulic model can adequately simulate the thermal behavior of this EHA system, despite the difficulty of acquiring all the precise design parameters of the real system as evidenced by the agreement of the simulation results with the experimental data. While there may be slight inconsistencies in temperature fits at different pressure points in Case 1, this is primarily due to the complexities involved in determining parameters like heat transfer coefficients and specific heat capacities, which are not directly measurable in the actual EHA system, and these physical parameters vary with the operating conditions. However, the main purpose of the model is to predict the long-term or steady-state thermal behavior, and approximate estimates or rough calculations are more useful than very accurate simulations. As such, the model adequately captures the temperature trends within the EHA system, even in scenarios where exact parameter measurements pose challenges, thus serving its purpose effectively.

IV. DISCUSSION

High-temperature hydraulic oil under extreme operating conditions can lead to untold consequences. To predict the thermal behavior of the hydraulic pump, two cases are simulated based on a calibrated thermal-hydraulic model that can track the temperature trend. The simulation results of different ports of the hydraulic pump are shown in Fig. 12 and Table 4.

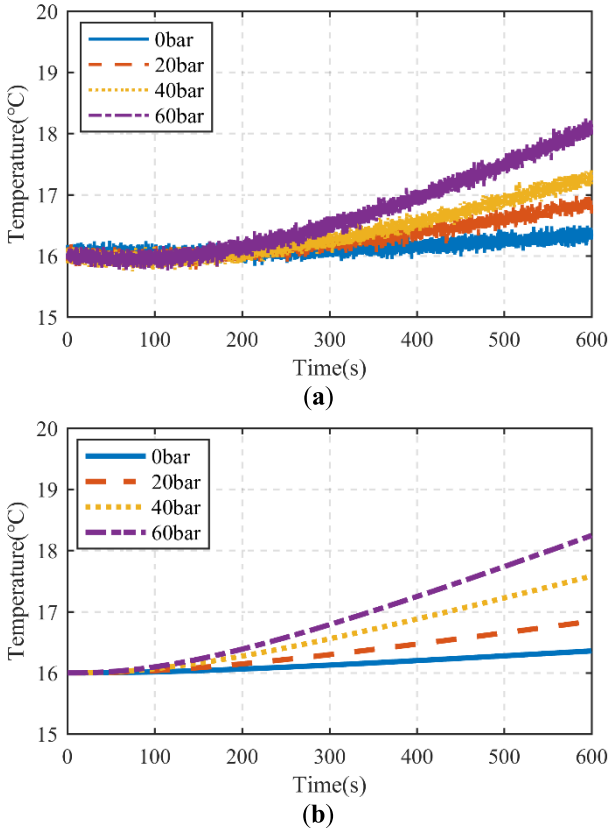

FIGURE 10. Measured temperature at different pressures (a) the experimental data; (b) the simulation data.

From the simulation results, it can be seen that the change is flat after about 200s. The highest temperature at the hydraulic pump drain port is attributed to the highest energy dissipation of the oil leakage; because of the spatial proximity to each other and the hydraulic oil cycles inside the closed system, the temperature of the inlet and outlet port is very close to each other, which is reasonable. In Case 1, the temperature of the drain port under 60 bar is close to the permissible temperature of 60°C, which may damage the system in the long term. In Case 2, the oil temperature fluctuates according to the system state, and the heat dissipation and power loss of the system are in balance after 200s. The limitations imposed by power availability and installation space pose significant challenges to effective heat dissipation. We must consider the extreme operating conditions for appropriate thermal design to guide the evaluation of the EHA.

A. AIR-COOLING DISSIPATION

EHAs find widespread application in aircraft control systems, such as rudder surfaces. In aircraft, ram air serves as an accessible heat source. The injection of outside air through the ram air intake can effectively cool aircraft components, such as electronic equipment, as shown in Fig. 13. Typically, ram air flow paths are strategically placed within the fuselage or wing, and EHAs in these areas can be utilized without complex structures. Therefore, in this paper, we refer to the reference [30] and investigate the performance of ram-air-cooling EHAs at different velocities.

TABLE 4. Simulation temperature of hydraulic pump ports at 600s.

Pressure(bar)	Position	Temperature (°C)
60	Inlet port	53.00
	Outlet port	54.17
	Drain port	59.67

TABLE 5. Simulation results at different velocities.

Velocity (m/s)	Convective exchange coefficient ($W/m^2/°C$)	Pump shell(°C)	Drain port(°C)
0	1.40	25.38	59.67
15	66.13	24.78	59.14
30	115.13	24.32	58.84
50	173.25	23.82	58.57

In the simulation results presented in Table 5, we observe that the heat transfer coefficient increases with rising velocities. Meanwhile, the temperature of both the hydraulic pump case and the drain port exhibits a decrease, albeit modest: 1.56°C and 1.1°C, respectively. Notably, the trend of this change remains inconspicuous. These observations can be attributed to the relatively small heat transfer area of the hydraulic pump and the substantial thermal resistance posed by the valve block. Consequently, achieving significant temperature reduction becomes challenging. However, it is essential to recognize that the utilization of ram air may result in decreased aircraft thrust and overall flight performance.

B. PHASE CHANGE DISSIPATION

Modern advanced aircraft with significant aerodynamic profiles and high stealth, flight Mach number reaches above 3 the ram air temperature will reach 300°C cannot be used for air cycle cooling [31]. The fuel oil used in traditional heat exchangers as the main component of the onboard heat sink means that the available heat sink becomes less with flight time, and high fuel oil temperatures also lead to a reduction in the amount of available heat sink. Liquefied natural gas (LNG) has the advantages of high latent heat of vaporization per unit mass, low vaporization temperature, and non-toxic and non-corrosive properties. Additionally, LNG is combustible and can potentially provide thrust or power to the aircraft when required, there is significant potential as a novel type of available heat sink in further hypersonic aircraft [32].

Heat radiator performance is assessed in terms of the number of heat transfer units (NTU) determined by the heat capacity ratio and efficiency together, expressed as

$$NTU = \frac{k_c A_U}{\min(\dot{m}_1 c_{p1}, \dot{m}_2 c_{p2})} \tag{20}$$

$$\eta_c = 1 - \exp\left\{\frac{NTU^{0.22}}{C^*}[\exp(-C^* NTU^{0.78}) - 1]\right\} \tag{21}$$

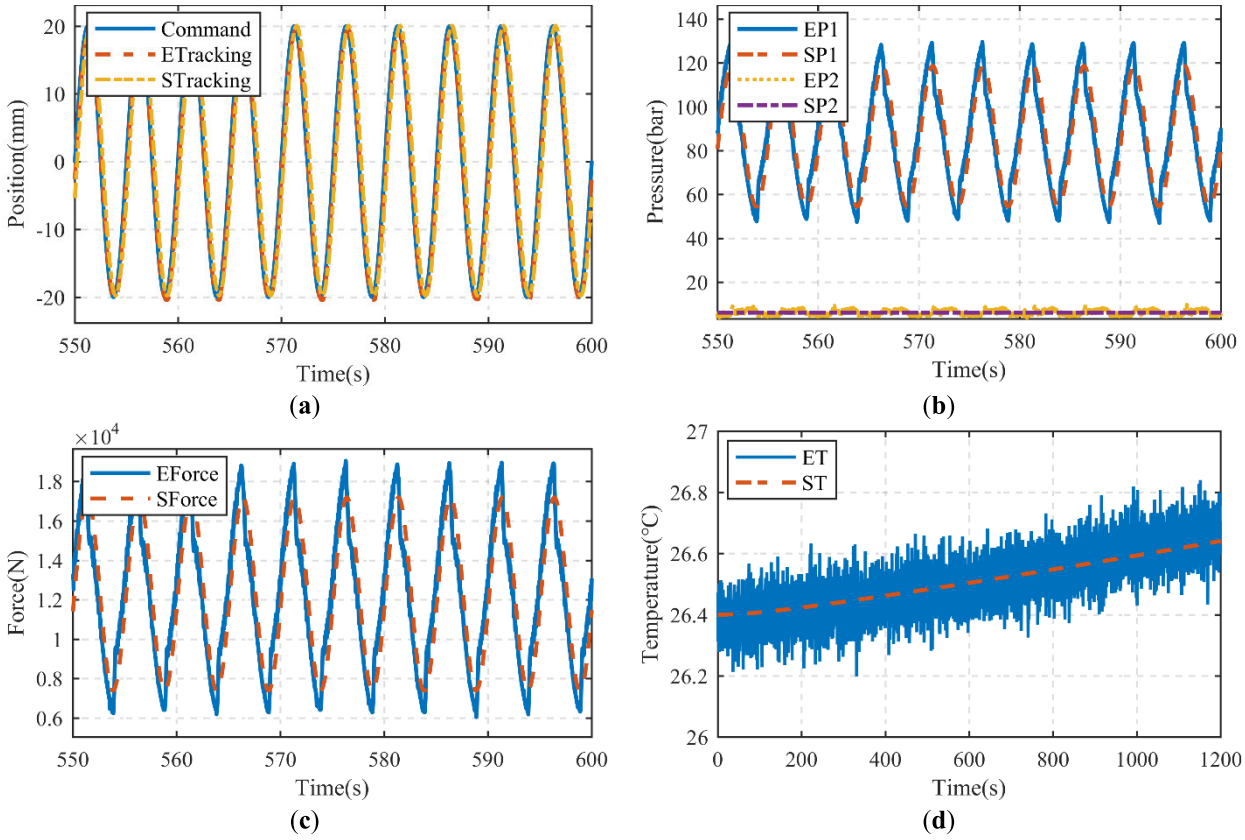

FIGURE 11. The comparison between the experimental data and simulation results under the sinusoidal command: (a) tracking curve; (b) pressure curve, P1 is the high-pressure chamber pressure and P2 is the low-pressure chamber pressure; (c) load force curve; (d) measured temperature. 'E' is the experimental data and 'S' is the simulation data.

$$\phi_c = \eta_c \min(\dot{m}_1 c_{p1}, \dot{m}_2 c_{p2})(T_1' - T_2') \tag{22}$$

where k_c is the total heat transfer coefficient; A_U is the heat transfer area; $\dot{m}_1$ and $\dot{m}_2$ are the mass flow rates, $c_{p1,}$ and c_{p2} are the specific heat capacity; η_c is heat transfer efficiency; C^* is the heat capacity ratio, and $T_1^{'}$ and $T_2^{'}$ indicate the inlet and outlet temperatures of the cold side.

To consider the feasibility of LNG in terms of volume and weight after the introduction of the thermal management system, the following evaluation calculation is required: Based on the overall operating parameters, the total mass of LNG required when the heat sink is equal to the heat produced by the heat source is calculated.

$$Q_{LNG} = P_{sum} t_m \tag{23}$$

$$Q_{LNG} = (c_{p,LNG,latent} + c_{p,LNG,sensible} \Delta T_{LNG}) M_{LNG} \tag{24}$$

$$M_{LNG} = V_{LNG} \rho_{LNG} \tag{25}$$

where Q_{LNG} is the heat sink; P_{sum} is the heat power; t_m is the mission time; $c_{p,LNG,latent}$, laterer is the latent heat value of vaporization of LNG, $c_{p,LNG,sensible}$ LNG sensible is the sensible specific heat capacity of LNG, ΔT_{LNG} is the temperature difference between import and export of LNG. M_{LNG} is the total mass of LNG; V_{LNG} is the total volume of LNG; ρ_{LNG} is the density of LNG. The values of the simulation parameters are shown in Table 6.

TABLE 6. Parameters of the simulation model.

Parameter	Value	Parameter	Value
$c_{p,\mathrm{LNG},latent}$	509kJ/kg	$c_{p,\mathrm{LNG},sensible}$	2.9kJ/kg
ΔT_{LNG}	180°C	ρ_{LNG}	430kg/m^3

In Case 1 the power loss at 60 bar pressure is 0.7 kW and the combined system thermal power is about 1.5 kW. The needed LNG is 2.3 L. Considering a twofold redundancy for safety, the volume of LNG is increased to 5 L, which corresponds to a mass of approximately 2.15 kg. The radiator is arranged in the return line after the actuator, and the switching valve is opened to dissipate the heat when the temperature is greater than 40°C. The simulation results are shown in Fig. 15.

The simulation results show that the temperature of the drain port of the hydraulic pump is kept below 50°C at all times. When the circulating oil temperature approaches the critical threshold at approximately 110s, the LNG valve autonomously opens to initiate additional cooling measures. This process helps regulate the temperature of the circuit in conjunction with the inherent heat dissipation capabilities of the system. The maximum temperature of the hydraulic

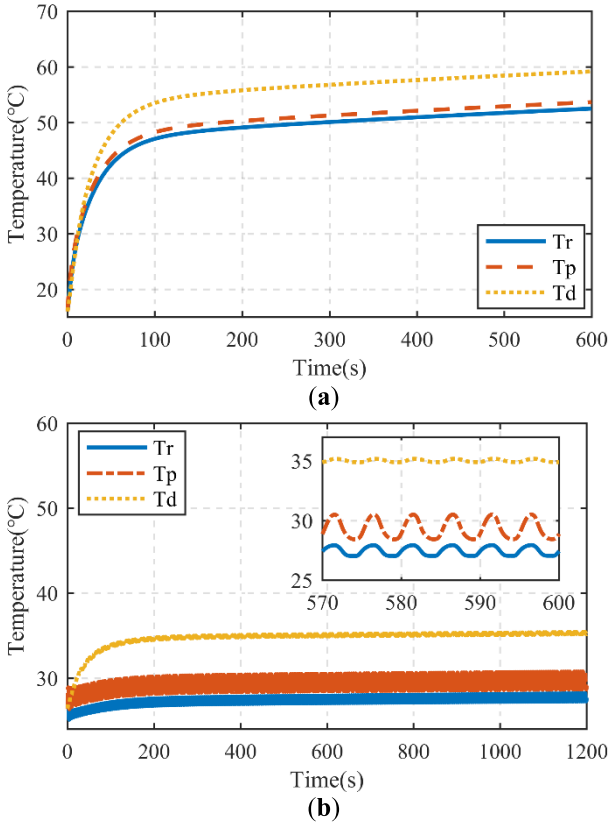

FIGURE 12. Simulation results of the hydraulic pump. (a) Pressure 60 bar in Case 1; (b) Case 2. 'Tr' is the inlet port temperature, 'Tp' is the outlet port temperature, and 'Td' is the drain port temperature.

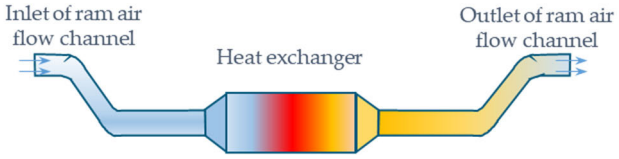

FIGURE 13. Structure of the ram airflow channel.

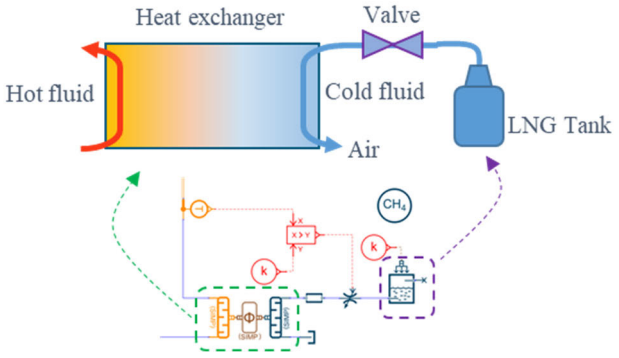

FIGURE 14. Heat radiator structure and the simulation model.

system is controlled below the temperature limit for efficient thermal management of the EHA.

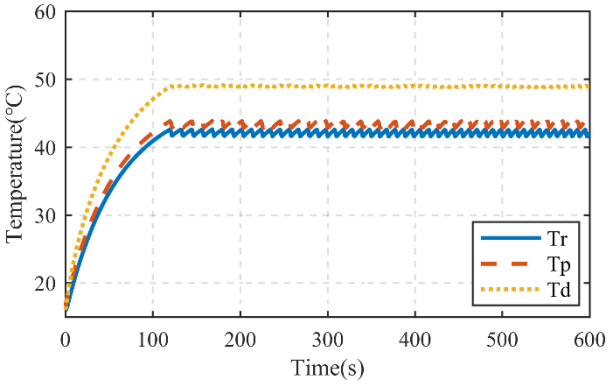

FIGURE 15. Simulation results of the hydraulic pump with heat dissipation.

V. CONCLUSION

In this study, the power loss and heat dissipation characteristics of EHA during the energy transfer process to address thermal management system challenges. A one-dimensional simulation model of the EHA thermal-hydraulic system is established. Through a comparison between simulation results and experimental data from an operational EHA system, the agreement between the simulation and the experimental results confirms that the developed model can accurately simulate the thermal behavior of the EHA. Based on the validation of the model, the study delves into exploring the cooling strategy for the EHA. Various cooling mechanisms such as air-cooling and phase-change heat dissipation are evaluated, and a heat sink utilizing LNG as a consumable cooling source is designed to meet the overall design requirements. Simulation result verifies the feasibility of the proposed cooling scheme, offering a novel solution to mitigate overheating in EHA system for high-speed aircraft applications. In future work, we will explore more scenarios used for this EHA system to further improve the modeling approach and experimentally investigate different thermal management architectures.

REFERENCES

[1] M. Kumar, "A survey on electro hydrostatic actuator: Architecture and way ahead," *Mater. Today: Proc.*, vol. 45, pp. 6057–6063, Jan. 2021, doi: 10.1016/j.matpr.2020.10.049.

[2] V. Nicolae, C.-G. Toma, C. Constantin, V. Daniela, and B. M. Daniel, "Modeling and simulation of a hybrid electrohydraulic flight control servomechanism for A380," in *Proc. 7th Int. Conf. Comput. Commun. Control (ICCCC)*, May 2018, pp. 150–155, doi: 10.1109/ICCCC.2018.8390452.

[3] W. Chen, T. Lin, B. P. Hill, and J. R. Brown, "Thermal modelling of a flight-critical electrohydrostatic actuator," *SAE Trans.*, vol. 104, pp. 233–246, May 1995.

[4] M. T. Nguyen, T. D. Dang, and K. K. Ahn, "Application of electro-hydraulic actuator system to control continuously variable transmission in wind energy converter," *Energies*, vol. 12, no. 13, p. 2499, Jun. 2019.

[5] H. Kwon and M. Ivantysynova, "Experimental and theoretical studies on energy characteristics of hydraulic hybrids for thermal management," *Energy*, vol. 223, May 2021, Art. no. 120033, doi: 10.1016/j.energy.2021.120033.

[6] X. Guo and A. Vacca, "Advanced design and optimal sizing of hydrostatic transmission systems," *Actuators*, vol. 10, no. 9, p. 243, Sep. 2021, doi: 10.3390/act10090243.

[7] J. Mattila, J. Koivumäki, D. G. Caldwell, and C. Semini, "A survey on control of hydraulic robotic manipulators with projection to future trends," *IEEE/ASME Trans. Mechatronics*, vol. 22, no. 2, pp. 669–680, Apr. 2017, doi: 10.1109/TMECH.2017.2668604.

[8] M. Sun, X. Ouyang, J. Mattila, Z. Chen, H. Yang, and H. Liu, "Lightweight electrohydrostatic actuator drive solution for exoskeleton robots," *IEEE/ASME Trans. Mechatronics*, vol. 27, no. 6, pp. 4631–4642, Dec. 2022, doi: 10.1109/TMECH.2022.3153706.

[9] A. S. J. van Heerden, D. M. Judt, S. Jafari, C. P. Lawson, T. Nikolaidis, and D. Bosak, "Aircraft thermal management: Practices, technology, system architectures, future challenges, and opportunities," *Prog. Aerosp. Sci.*, vol. 128, Jan. 2022, Art. no. 100767, doi: 10.1016/j.paerosci.2021.100767.

[10] Z. Ma, H. Liao, J. Gao, S. Nie, and Y. Geng, "Physics-informed machine learning for degradation modeling of an electro-hydrostatic actuator system," *Rel. Eng. Syst. Saf.*, vol. 229, Jan. 2023, Art. no. 108898, doi: 10.1016/j.ress.2022.108898.

[11] S. Nie, J. Gao, Z. Ma, F. Yin, and H. Ji, "An online data-driven approach for performance prediction of electro-hydrostatic actuator with thermal-hydraulic modeling," *Rel. Eng. Syst. Saf.*, vol. 236, Jan. 2023, Art. no. 109289.

[12] X. U. Jinquan, J. I. N. Wenbo, G. U. O. Hong, and Y. U. Tian, "Modeling and analysis of oil frictional loss in wet-type permanent magnet synchronous motor for aerospace electro-hydrostatic actuator," *Chin. J. Aeronaut.*, vol. 36, no. 11, pp. 328–341, 2023.

[13] Z. Jiao, Y. Li, T. Yu, C. Jiang, L. Huang, and Y. Shang, "Dynamic thermal coupling modeling and analysis of wet electro-hydrostatic actuator," *Chin. J. Aeronaut.*, vol. 35, no. 6, pp. 298–311, Jun. 2022, doi: 10.1016/j.cja.2021.04.007.

[14] Q. Chao, J. Zhang, B. Xu, Y. Shang, Z. Jiao, and Z. Li, "Load-sensing pump design to reduce heat generation of electro-hydrostatic actuator systems," *Energies*, vol. 11, no. 9, pp. 1–13, 2018.

[15] Z. Song, Z. Jiao, Y. Shang, S. Wu, and W. Hu, "Design and analysis of a direct load sensing electro-hydrostatic actuator," in *Proc. Int. Conf. Fluid Power Mechatronics (FPM)*, Aug. 2015, pp. 624–627, doi: 10.1109/FPM.2015.7337190.

[16] L. Huang, T. Yu, Z. Jiao, and Y. Li, "Active load-sensitive electro-hydrostatic actuator for more electric aircraft," *Appl. Sci.*, vol. 10, no. 19, p. 6978, Oct. 2020, doi: 10.3390/app10196978.

[17] M. Yang, G. Yan, Y. Zhang, T. Zhang, and C. Ai, "Research on high efficiency and high dynamic optimal matching of the electro-hydraulic servo pump control system based on NSGA-II," *Heliyon*, vol. 9, no. 3, Mar. 2023, Art. no. e13805, doi: 10.1016/j.heliyon.2023.e13805.

[18] Y. Shang, X. Li, H. Qian, S. Wu, Q. Pan, L. Huang, and Z. Jiao, "A novel electro hydrostatic actuator system with energy recovery module for more electric aircraft," *IEEE Trans. Ind. Electron.*, vol. 67, no. 4, pp. 2991–2999, Apr. 2020, doi: 10.1109/TIE.2019.2905834.

[19] X. Han, T. Minav, M. Wang, Y. Fu, and M. Pietola, "Thermal coupling simulation of electro-hydrostatic actuator subjected to critical temperature conditions," *Int. J. Fluid Power*, vol. 23, no. 9, pp. 379–394, Sep. 2022, doi: 10.13052/ijfp1439-9776.2336.

[20] H. Yang, D. Ren, X. Yang, W. Lin, and B. Liu, "Thermal-hydraulic modeling and simulation of the electro-hydrostatic actuator hydraulic system based on lumped-parameter method," in *Proc. 9th Int. Symp. Syst. Secur., Saf., Rel. (ISSSR)*, Jun. 2023, pp. 361–368, doi: 10.1109/isssr58837.2023.00060.

[21] G. Yan, Z. Jin, M. Yang, and B. Yao, "The thermal balance temperature field of the electro-hydraulic servo pump control system," *Energies*, vol. 14, no. 5, p. 1364, Mar. 2021, doi: 10.3390/en14051364.

[22] S. Qu, D. Fassbender, A. Vacca, and E. Busquets, "Development of a lumped-parameter thermal model for electro-hydraulic actuators," in *Proc. 10th Int. Conf. Fluid Power Transmiss. Control*, Apr. 2021, pp. 1–12.

[23] S. Ketelsen, S. Michel, T. O. Andersen, M. K. Ebbesen, J. Weber, and L. Schmidt, "Thermo-hydraulic modelling and experimental validation of an electro-hydraulic compact drive," *Energies*, vol. 14, no. 9, p. 2375, Apr. 2021, doi: 10.3390/en14092375.

[24] D. van den Bossche, "The A380 flight control electrohydrostatic actuators," in *Proc. 25Th Int. Congr. Aeronaut. Sci.*, 2006, pp. 1–8.

[25] G. Lenoble, M. Olivier, A. Steblinkin, D. Donjat, and A. Jimenez, "Elevator actuator housing bay flight mission thermal integrated analysis," in *Recent Adv. Aerosp. Actuation Syst. Compon. (R3ASC) Conf. Proc.*, 2016, pp. 118–126.

[26] Y. Li, H. Han, M. Li, J. Zhang, Y. Xing, S. Lei, and X. Yu, "Multi-objective optimization of a novel ribbed honeycomb heat sink for an electro-hydrostatic actuator," *Processes*, vol. 11, no. 9, p. 2526, Aug. 2023, doi: 10.3390/pr11092526.

[27] Z. Rehman and K. Seong, "Three-D numerical thermal analysis of electric motor with cooling jacket," *Energies*, vol. 11, no. 1, p. 92, Jan. 2018, doi: 10.3390/en11010092.

[28] K. Gao, Y. Fu, J. Zhao, S. Wang, and J. Fu, "Thermal analysis and simulation for EHA hydraulic piston pump," *Chin. Intell. Syst. Conf.*, vol. 803, pp. 874–883, 2022, doi: 10.1007/978-981-16-6328-4_87.

[29] E. Busquets and M. Ivantysynova, "Temperature prediction of displacement controlled multi-actuator machines," *Int. J. Fluid Power*, vol. 14, no. 1, pp. 25–36, Jan. 2013, doi: 10.1080/14399776.2013.10781066.

[30] W. Lian, J. Zhang, and H. Wan, "Numerical research on the cooling performance of an aircraft electromechanical actuator based on heat pipes-fuel and heat pipes-ram air cooling conception," *Adv. Mech. Eng.*, vol. 14, no. 5, May 2022, Art. no. 168781322210969, doi: 10.1177/16878132221096965.

[31] Y.-F. Mao, Y.-Z. Li, J.-X. Wang, K. Xiong, and J.-X. Li, "Cooling ability/capacity and exergy penalty analysis of each heat sink of modern supersonic aircraft," *Entropy*, vol. 21, no. 3, p. 223, Feb. 2019, doi: 10.3390/e21030223.

[32] C. Cheng, P. Yu, Z. Xie, Y. Li, and Z. Jiao, "Design simulation and analysis of TMS for hypersonic aircraft based on LNG," *Acta Aeronautica Astronautica Sinica*, vol. 44, no. 10, 2022, Art. no. 127545.

JIAHUI LIU received the B.S. degree in mechanical engineering from Nanjing University of Science and Technology, Nanjing, China, in 2018, where he is currently pursuing the Ph.D. degree.

His current research interests include servo control of electro-hydrostatic systems, intelligent monitoring, and characterization of mechatronic systems.

HAO HUANG received the B.Eng. degree from Nanjing University of Science and Technology (NJUST), China, in 2021, where he is currently pursuing the master's degree in mechanical engineering with the Sino-French Engineer School.

His research interest includes thermal analysis of electro-hydrostatic systems.

YAOWEN GE received the Ph.D. degree from Nanjing University of Science and Technology (NJUST), China, in 2023. He is currently a Postdoctoral Researcher with NJUST.

His research interest includes electro-hydrostatic actuator modeling and control.

XIAOLI ZHAO received the M.S. degree from Lanzhou University of Technology, Lanzhou, China, in 2017, and the Ph.D. degree in mechanical engineering from the School of Mechanical Engineering, Southeast University, Nanjing, China, in 2021.

From September 2019 to September 2020, he was a Visiting Ph.D. Researcher with the School of Engineering, The University of British Columbia, Okanagan Campus, Canada. He is currently an Assistant Professor with the School of Mechanical Engineering, Nanjing University of Science and Technology, Nanjing. His main research interests include intelligent monitoring and fault diagnosis, prognostic and health management for electromechanical and hydraulic systems, artificial intelligence, signal processing, and rehabilitation robots.

WENXIANG DENG received the B.Tech. degree in mechanical engineering from Central South University, Changsha, China, in 2013, and the Ph.D. degree in mechanical engineering from Nanjing University of Science and Technology (NJUST), Nanjing, China, in 2018.

He is currently a Lecturer with the School of Mechanical Engineering, NJUST. His current research interests include servo control of mechatronic systems, hydraulic robot control, robust adaptive control, and nonlinear compensation.

GUANGFA GAO received the Ph.D. degree from the University of Science and Technology of China (USTC), in 2010. From January 2011 to June 2013, he was a Postdoctoral Fellow with the Department of Modern Mechanics, USTC, and an Associate Professor with the Department of Safety Science and Engineering, Anhui University of Science and Technology (AUST). From June 2013 to January 2016, he was a Researcher with the Laboratory of Impact Engineering/Center for Protective Technologies (LIP/CPT), National University of Singapore (NUS). In 2015, he joined the School of Mechanical Engineering, Nanjing University of Science and Technology, where he is currently a Full Professor. His current research interests include solid mechanics, engineering mechanics, munitions engineering, blast and impact dynamics, endpoint ballistic effects, and safety protection technology and engineering.

JIANYONG YAO (Member, IEEE) received the B.Tech. degree in mechatronics from Tianjin University, Tianjin, China, in 2006, and the Ph.D. degree in mechatronic engineering from Beihang University, Beijing, China, in 2012.

From October 2010 to October 2011, he was a Visiting Exchange Student with the School of Mechanical Engineering, Purdue University, West Lafayette, IN, USA. In 2012, he joined the School of Mechanical Engineering, Nanjing University of Science and Technology, Nanjing, China, where he is currently a Full Professor. His current research interests include servo control of mechatronic systems, adaptive and robust control, fault detection, and accommodation of dynamic systems.